ACS NANO

www.acsnano.org

ARTICLE

Open Resonator Electric Spaser

Bobo Liu,[†] Weiren Zhu,[‡] Sarath D. Gunapala,[§] Mark I. Stockman,[#] and Malin Premaratne*[,†]

[†]Advanced Computing and Simulation Laboratory (AχL), Department of Electrical and Computer Systems Engineering, Monash University, Clayton, Victoria 3800, Australia

[‡]Department of Electronic Engineering, Shanghai Jiao Tong University, Shanghai 200240, People's Republic of China

[§]Jet Propulsion Laboratory, California Institute of Technology, Pasadena, California 91109, United States

[#]Center for Nano-Optics and Department of Physics and Astronomy, Georgia State University, Atlanta, Georgia 30303, United States

Supporting Information

ABSTRACT: **The inception of the plasmonic laser or spaser (surface plasmon amplification by stimulated emission of radiation) concept in 2003 provides a solution for overcoming the diffraction limit of electromagnetic waves in miniaturization of traditional lasers into the nanoscale. From then on, many spaser designs have been proposed. However, all existing designs use closed resonators. In this work, we use cavity quantum electrodynamics analysis to theoretically demonstrate that it is possible to design an electric spaser with an open resonator or a closed resonator with much weak feedback in the extreme quantum limit in an all-carbon platform. A carbon nanotube quantum dot plays the role of a gain element, and Coulomb blockade is observed. Graphene nanoribbons are used as the resonator, and surface plasmon polariton field distribution with quantum electrodynamics features can be observed. From an engineering perspective, our work makes preparations for integrating spasers into nanocircuits and/or photodynamic therapy applications.**

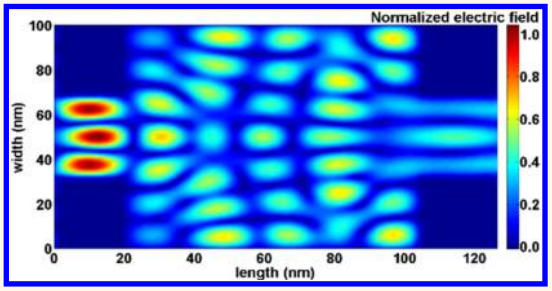

KEYWORDS: *spaser, graphene, Coulomb blockade, carbon nanotube, plasmon*

In nanoplasmonics, the spaser (surface plasmon amplification by stimulated emission of radiation) is a promising quantum generator that can overcome fundamental problems brought by miniaturization beyond the diffraction limit imposed on electromagnetic waves.[1,2] A spaser is a nanoplasmonic counterpart of the laser, consisting of a plasmonic oscillator coupled to an active (gain) medium, which was proposed by Bergman and Stockman in 2003.[3−5] Since then, different spaser architectures and material compositions are proposed and analyzed to satisfy various needs in applications.[4−23] In 2010, the spasers based on noble metals were investigated as both a nanoscale quantum generator and an ultrafast amplifier by employing a quantum kinetic theory and density matrix equations.[17] In recent years, Rupasinghe *et al.*[18] proposed an all-carbon spaser design, where a graphene nanoflake (GNF) resonator was coupled to a carbon nanotube (CNT) gain element, which was optically pumped. This work proved that continuous spasing can be sustained on a predominantly carbon platform provided material and geometrical parameters are judicially selected. Rupasinghe et al. calculated the transition energy and relaxation rates of the gain element using a tight-binding model which generated the band structure and associated density of states. However, they limited their study to plasmonic wave modes excitable in a closed graphene nanoflake resonator. Another graphene based electric spaser was proposed by Apalkov *et al.*,[19] in which, the gain medium employed a semiconductor cascade quantum well structure. The closed resonator was made by a graphene nanopatch. This work showed that spasing in an electrically pumped graphene resonator can be achieved with careful selection of parameters. Moreover, an electric spaser in the extreme quantum limit was theoretically investigated by Li *et al.*[23] It showed that an electric spaser with a gain element of a single-conductance quantum nanowire and a core of common plasmonic metals is fundamentally possible.

One thing common for existing spaser designs is that the oscillators are closed resonators.[3−23] So an important question arises of whether spasing can be built in an open resonator (or a closed resonator with much weak feedback) that is connected to plasmonic waveguides, which makes it possible for spasers to be integrated with nanocircuits and nanosystems. This is the primary task of our work. Also we note that a spaser as a nanoscale quantum generator and an ultrafast amplifier have been analyzed using quantum kinetic theory and density matrix equations, in which the temporal behavior of a spaser was investigated without looking at the spatial characteristics.[17] Moreover, the emission energy and polarization-relaxation rate of the gain elements are important parameters in spaser design,

Received: September 21, 2017
Accepted: October 31, 2017
Published: October 31, 2017

DOI: 10.1021/acsnano.7b06735
ACS Nano 2017, 11, 12573−12582

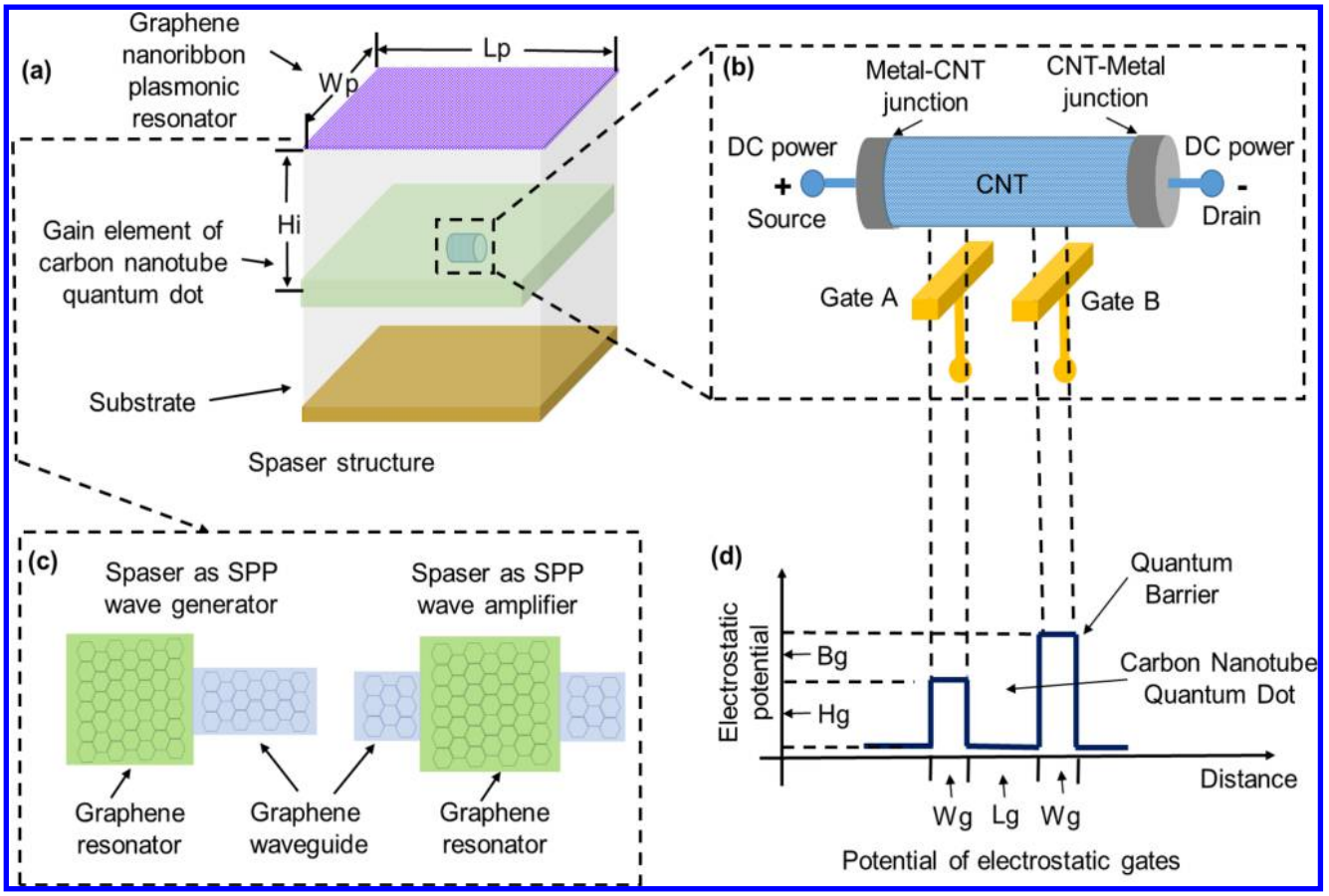

Figure 1. Structure of electric all-carbon spaser. (a) Architecture of the electric spaser. The graphene nanoribbon plasmonic resonator on the top layer is coupled with the gain subsystem consisting of carbon nanotube quantum dots under the resonator. The size of the plasmonic resonator is Wp × Lp; the distance between the resonator and gain elements array is Hi. The bottom layer is the substrate. (b) Electric spaser gain element made from carbon nanotube quantum dot. Gates A and B control the electrostatic potential of the quantum barrier. (c) Left: Graphene nanoribbon plasmonic resonator of the electric spaser as the generator. Right: Graphene nanoribbon plasmonic resonator of the electric spaser as the amplifier. The waveguide of the SPPs is connected to the resonator. (d) Electrostatic potential profile of the carbon nanotube quantum dot as the gain elements of the electric spaser. Lg is the length of the quantum dot, Wg is the width of the quantum barrier, Hg is the height of the quantum barrier, and Bg is the bias between gates A and B due to the source−drain voltage drop.

but their quantitative dependence on the conductance of gain elements, quantum dot size, and bias voltage has not been revealed in existing electric spaser designs,[3−23] so a detailed first-principle method to improve the existing models is also in demand. Additionally, plasmonic metals are the focus of attention in the study of electric spasers under extreme quantum limit pumped by a ballistic single-conductance quantum nanowire; however, carbon materials such as graphene and carbon nanotube have not yet been studied on extreme ballistic spasers.[23]

Therefore, our work aims to explore these aforementioned problems by building an electric all-carbon spaser pumped by a ballistic single-conductance carbon nanotube quantum dot in the extreme quantum regime.[23] The graphene nanoribbon is used as the open resonator connecting to plasmonic waveguides. The spatial characteristics of both cases of plasmonic generators and amplifiers are studied. The spatial surface plasmon polariton (SPP) wave modes are obtained by solving the Helmholtz equation using mode-matching scattering matrix techniques.[24−32] The gain subsystem consists of a carbon nanotube quantum dot excited electrically.[33,34] The conductance, transition energy, and polarization-relaxation rate of the gain element are calculated using the atomistic basis tight-binding model and the nonequilibrium Green's function (NEGF) method.[24,25] Finally, the spasing conditions are investigated using quantum mechanical density matrix methods.[35]

This paper is organized as follows. The first section presents the overall design of the spaser. The physics of the gain medium and plasmonic resonator are covered in the next two sections. The spaser kinetics are analyzed next. The conclusion closes this paper, discussing the differences of this proposed device against existing devices, its significance, and potential value in applications. The detailed algorithms are presented in the Supporting Information.

RESULTS AND DISCUSSION

Overall Design of the Spaser. A carbon-based electric spaser in the extreme quantum limit is proposed in this work. The plasmonic resonator of this spaser is made from a graphene nanoribbon monolayer, and its active gain element is an electrically pumped carbon nanotube quantum dot. The graphene nanoribbons as waveguides are connected to the plasmonic resonator for transmission of SPP waves. The SPP modes are supported in the plasmonic resonator, and the gain medium is population inverted to supply energy to the plasmonic modes.

DOI: 10.1021/acsnano.7b06735
ACS Nano 2017, 11, 12573−12582

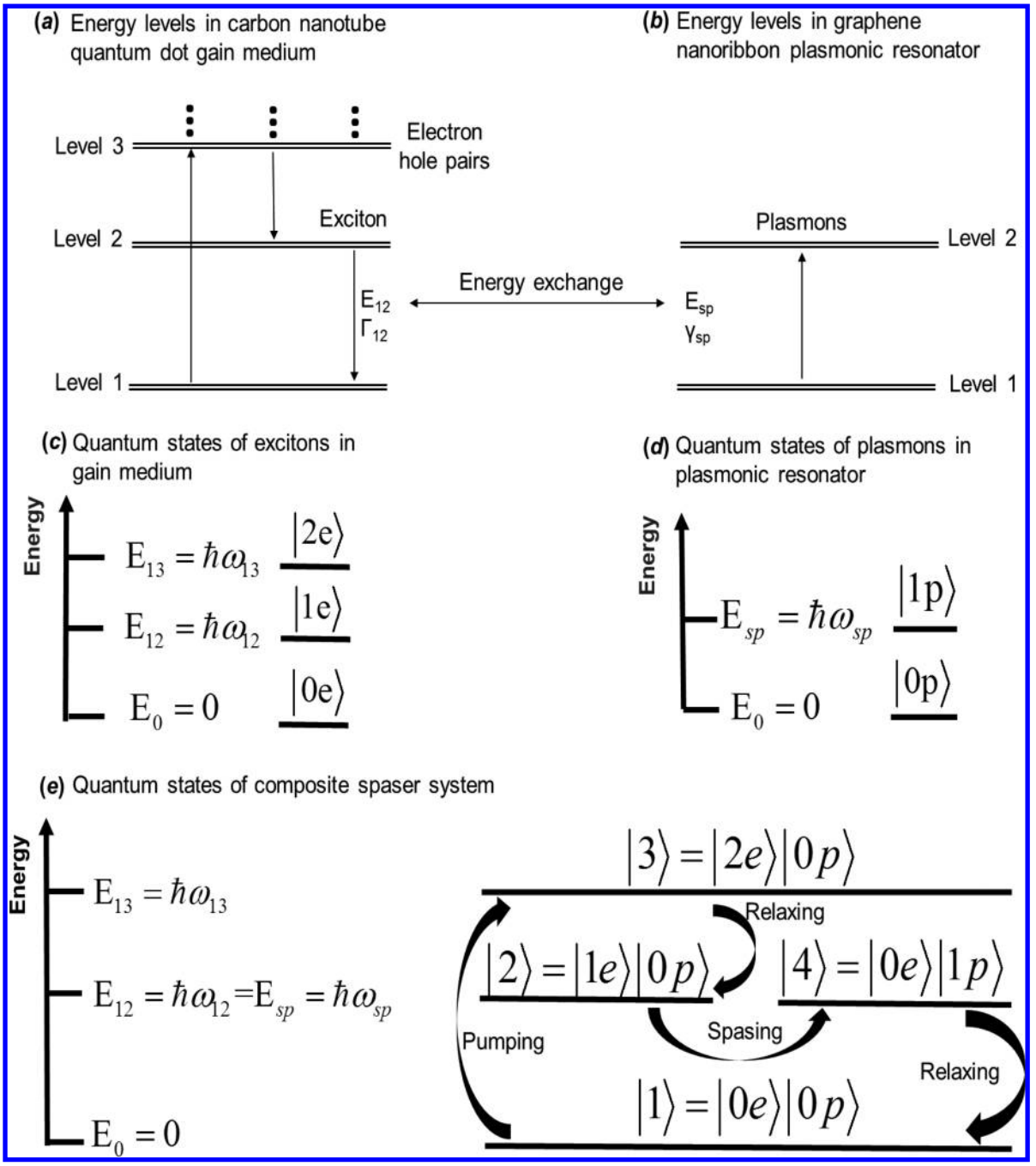

Figure 2. Energy levels and quantum states in an electric all-carbon spaser. (a) Energy levels of the carbon nanotube quantum dot gain element. Levels 1, 2, and 3 mark the subband energy levels in the carbon nanotube quantum dots. E_{12} and Γ_{12} are the intersubband transition energy and the gain element relaxation rate (spectral width). (b) Energy levels of the graphene nanoribbon plasmonic SPP. E_{sp} and γ_{sp} are the intersubband transition energy and the plasmon relaxation rate (spectral width). (c) Quantum states of excitons in the carbon nanotube quantum dot gain element. E_{12} and E_0 are the excited state and the ground state for the spasing process. (d) Quantum states of the graphene nanoribbon plasmonic SPP. E_{sp} and E_0 are the excited state and the ground state for the spasing process. (e) Quantum states of the composite electric spaser system, which is the product states of gain elements of the carbon nanotube quantum dots and the graphene nanoribbon plasmonic resonator SPP states.

Figure 1a illustrates the overall design of the proposed electric spaser. The graphene nanoribbon plasmonic resonator on the top layer is coupled with the gain subsystem consisting of a carbon nanotube quantum dot under the resonator. The size of the plasmonic resonator is Wp × Lp, and the distance between the resonator and gain element is Hi. The bottom layer is the substrate. Figure 1b shows the electric spaser gain element made from the carbon nanotube quantum dot, and the gates A and B control the electrostatic potential of the quantum barrier. The voltage drop between the source and drain is supplied by the dc power, which provides electrical injection of electrons into the upper bands and extraction from lower bands. Figure 1c shows the graphene nanoribbon plasmonic resonator. Figure 1d plots the electrostatic potential profile of the carbon nanotube quantum dot as the gain element of the electric spaser. The quantum dot forms between the constraints

DOI: 10.1021/acsnano.7b06735
ACS Nano 2017, 11, 12573−12582

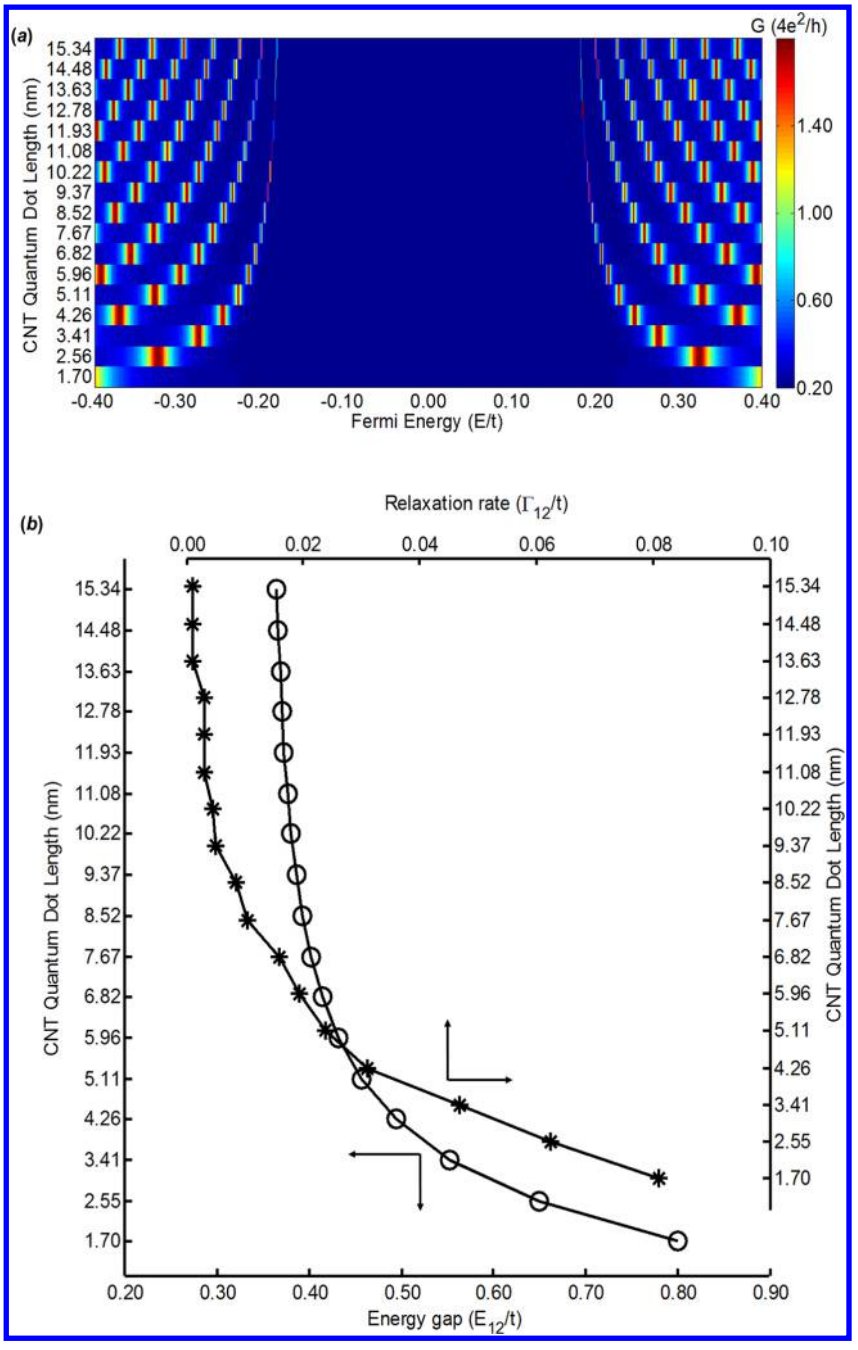

Figure 3. Conductance, energy gap, and relaxation rate in gain element. (a) Discretized conductance G (for holes (left side) and electrons (right side)) as a function of the Fermi energy E/t and the size (length) of the quantum dot Lg. The bias between gates A and B is Bg = 0; the height of the barriers is 0.5t. The width of gates A and B is Wg = 0.852 nm. The diameter of the carbon nanotube is 0.7829 nm. There are 10 carbon atoms in the circumference atom ring of the zigzag edge type CNT. (b) Bottom: Energy gap E_{12} between the bottom level of the conduction band and the top level of the valence band as a function of the length of the quantum dot. Top: Relaxation rate (broadening of the level) Γ_{12} as a function of the dot length. The bias between gates A and B is Bg = 0; the height of the barriers is 0.5t. The width of gates A and B is Wg = 0.852 nm. (The unit of conductance in (a) is $4e^2/h$, the number 4 considers both the valley and spin degeneracy. The Fermi energy, energy gap, and relaxation rate in (a), (b), and (c) are normalized by the first nearest hopping energy of the carbon nanotube, t = 2.8 eV.)

of a pair of quantum barriers. Lg is the length of the quantum dot, Wg is the width of the quantum barrier, Hg is the height of the quantum barrier, and Bg is the bias between gates A and B due to source−drain voltage drop.

Figure 2 presents the spasing processes in our proposed carbon electric spaser. In Figure 2a, levels 1 and 2 mark the lower and upper subband energy levels in carbon nanotube quantum dots. E_{12} and Γ_{12} are the intersubband transition energy and the gain element relaxation rate (spectral width). Figure 2b shows the energy levels of the graphene nanoribbon plasmonic SPP; E_{sp} and γ_{sp} are the intersubband transition energy and the plasmon relaxation rate (spectral width). Figure 2c shows the quantum states of excitons in the carbon nanotube quantum dot gain element; E_{12} and E_0 are the excited state and the ground state for the spasing process. Figure 2d gives the quantum states of the graphene nanoribbon plasmonic SPP; E_{sp} and E_0 are the excited state and the ground state for the spasing process. Figure 2e shows the

DOI: 10.1021/acsnano.7b06735
ACS Nano 2017, 11, 12573−12582

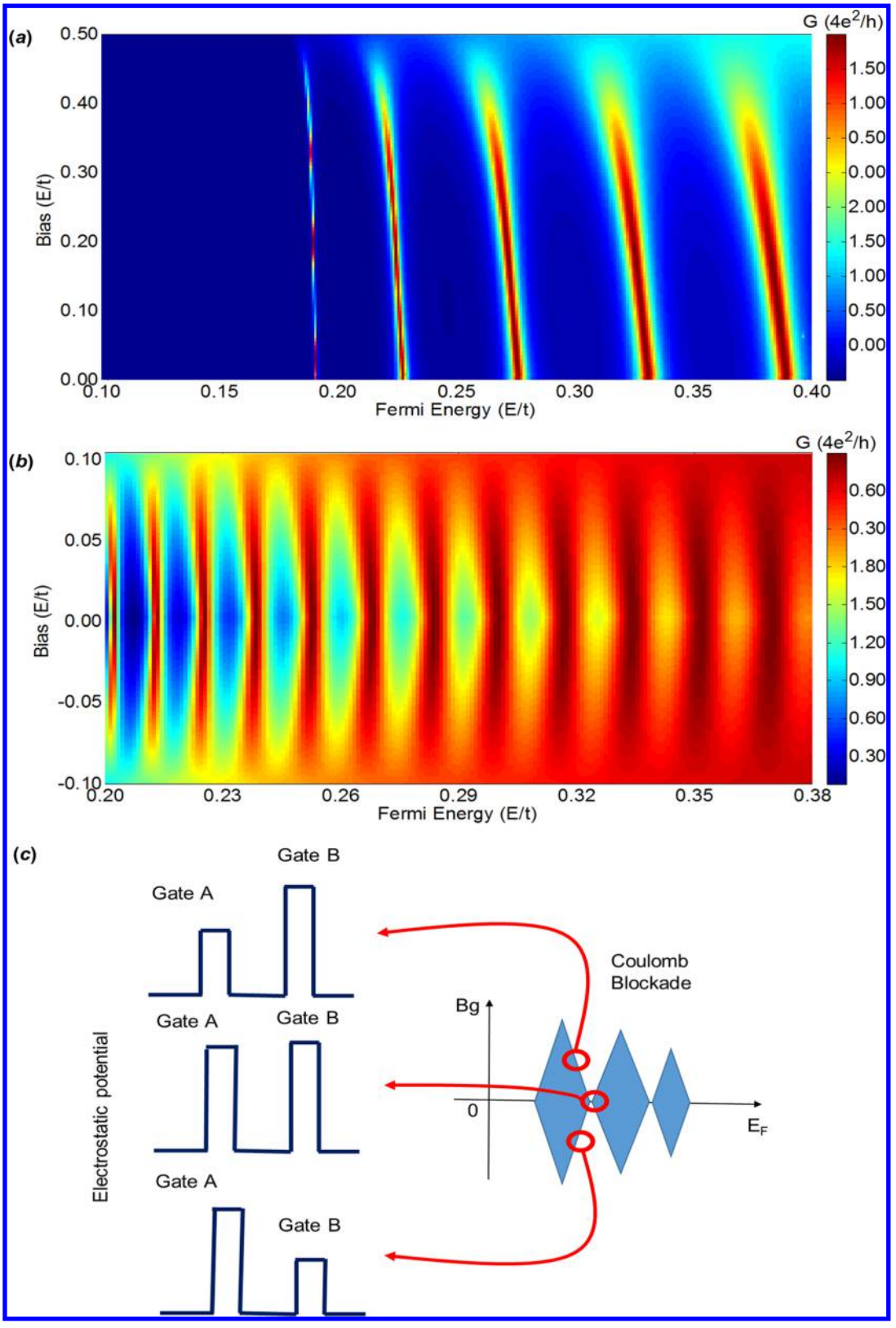

Figure 4. Coulomb blockade in the gain element. (a) Conductance G *vs* E/t and the bias Bg between gates A and B. The height of the barriers is 0.5t. The width of gates A and B is Wg = 0.852 nm. The length of the quantum dot is 10.22 nm. (b) Coulomb blockade (CB) *vs* Fermi energy (0.20−0.38 E/t) and bias potential. The length of the dot is 34.08 nm. The height of the barriers is 0.1t. The width of gates A and B is Wg = 0.852 nm. (c) Relation between the Coulomb blockade and the bias of the barriers. (The unit of conductance in (a) and (b) is $4e^2/h$; the number 4 considers both the valley and spin degeneracy. The Fermi energy and the bias in (a) and (b) are normalized by the first nearest hopping energy of the carbon nanotube, t = 2.8 eV.)

DOI: 10.1021/acsnano.7b06735
ACS Nano 2017, 11, 12573−12582

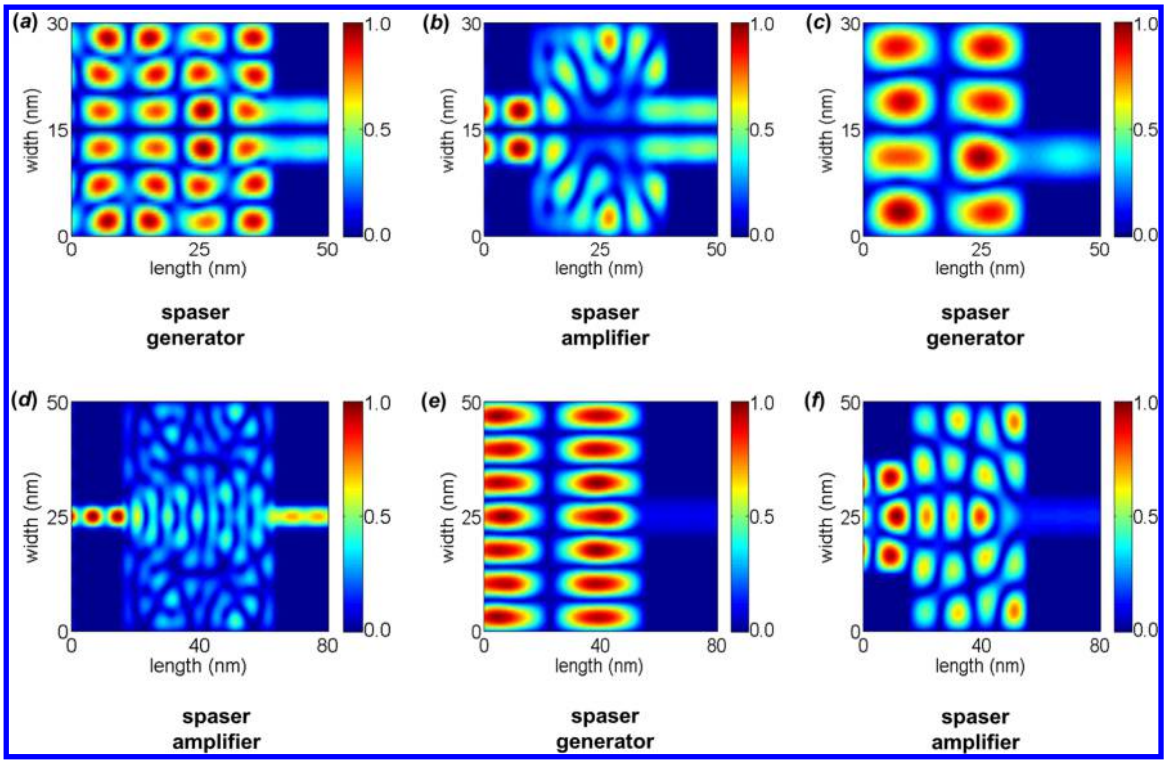

Figure 5. Normalized surface plasmon polariton (SPP) mode field distribution in the graphene nanoribbon plasmonic resonator in the electric spaser. The plasmon energy for (a), (b), and (d) is E(plasmon) = 0.460 × t (t = 2.8 eV). The plasmon energy for (c), (e), and (f) is E(plasmon) = 0.368 × t (t = 2.8 eV). The SPP modes propagate from left to right in (a)−(f).

quantum states of the composite electric spaser system, which is the product states of the gain element of the carbon nanotube quantum dot and the graphene nanoribbon plasmonic resonator SPP state. The carbon nanotube quantum dot is excited by the source and drain voltage drop together with electron (hole) injection and achieves population inversion. The electron and hole pairs are produced in the dot as depicted in Figure 2e. Then, the electron−hole pairs relax to form the excitons with an energy of E_{12} on level 2.

This transition is treated as a fast relaxation, so the gain elements are assumed as a two-level system. The excitons will recombine and drop to level 1 while emitting energy to the resonator surface plasmon depicted in Figure 2e. After that, the surface plasmonic oscillations in the graphene nanoribbon create the high local fields and excite the gain medium, stimulating the emission as a feedback. The feedback needs to be strong enough and the lifetime of the spaser SP mode needs to be long enough for building the stimulated emission. As shown in Figure 2, the condition $E_{12} = E_{sp}$ needs to be satisfied for spasing. Although the spaser has two different subsystems, the spaser operates as a single composite SPP generation device.

Physics of the Gain Medium. The gain medium is a carbon nanotube quantum dot excited by the injection of electrons and holes due to source and drain voltage drop. The conductance of the dot is calculated using the nonequilibrium Green's function formalism.[24,25] The influence of the contacts on the spaser system is incorporated using the terms of self-energies in the NEGF framework.[24,25] Detailed algorithms can be found in the Supporting Information.

Figure 3a illustrates the discretized conductance G (for holes (left side) and electrons (right side)) of the dot as a function of the Fermi energy E/t and the size (length) of quantum dot Lg. The emission energy E_{12}/t and the gain relaxation rate (spectral width Γ_{12}/t) extracted from the discretized conductance spectrum in Figure 3a are plotted in Figure 3b as a function of the length of the carbon nanotube dot on the bottom and top sides, respectively. It shows that both the emission energy E_{12}/t and the gain relaxation rate (spectral width Γ_{12}/t) increase as the length of the quantum dot decreases. Figure 4a presents the conductance of the quantum dot as a function of the Fermi energy and bias potential energy Bg. The height of the quantum barriers is 0.5t. Figure 4b presents the conductance of the quantum dot as a function of the Fermi energy and bias potential energy Bg. The height of the quantum barriers is 0.1t. The Coulomb blockade (CB) pattern can be observed here, boundaries of which are identified by some diamond markers shown in Figure 4c. The Coulomb blockade pattern reveals the single-electron-tunneling nature of the gain element and indicates that the energy gap between discretized levels will narrow and the spectral width will be broadened as the bias value is raised. Further details including an extensive analysis on the Coulomb blockade in nanostructures can be found elsewhere.[36−42]

Physics of the Open Plasmonic Resonator. The mode-matching scattering matrix technique is employed to solve the Helmholtz equation for SPP modes in the graphene plamonic resonator and waveguides.[24−34] The details of calculations are presented in the Supporting Information. The coupling between resonator and waveguides is considered in the calculations. The normalized electric field distributions of the SPP modes are presented in Figure 5a−f for both scenarios; spasers as plasmon generators and amplifiers. The width of the waveguides is tuned to support different numbers of transmission channels. The SPP propagates from left to right. The Fermi energy of the graphene nanoribbon is set to 10 meV,

DOI: 10.1021/acsnano.7b06735
ACS Nano 2017, 11, 12573−12582

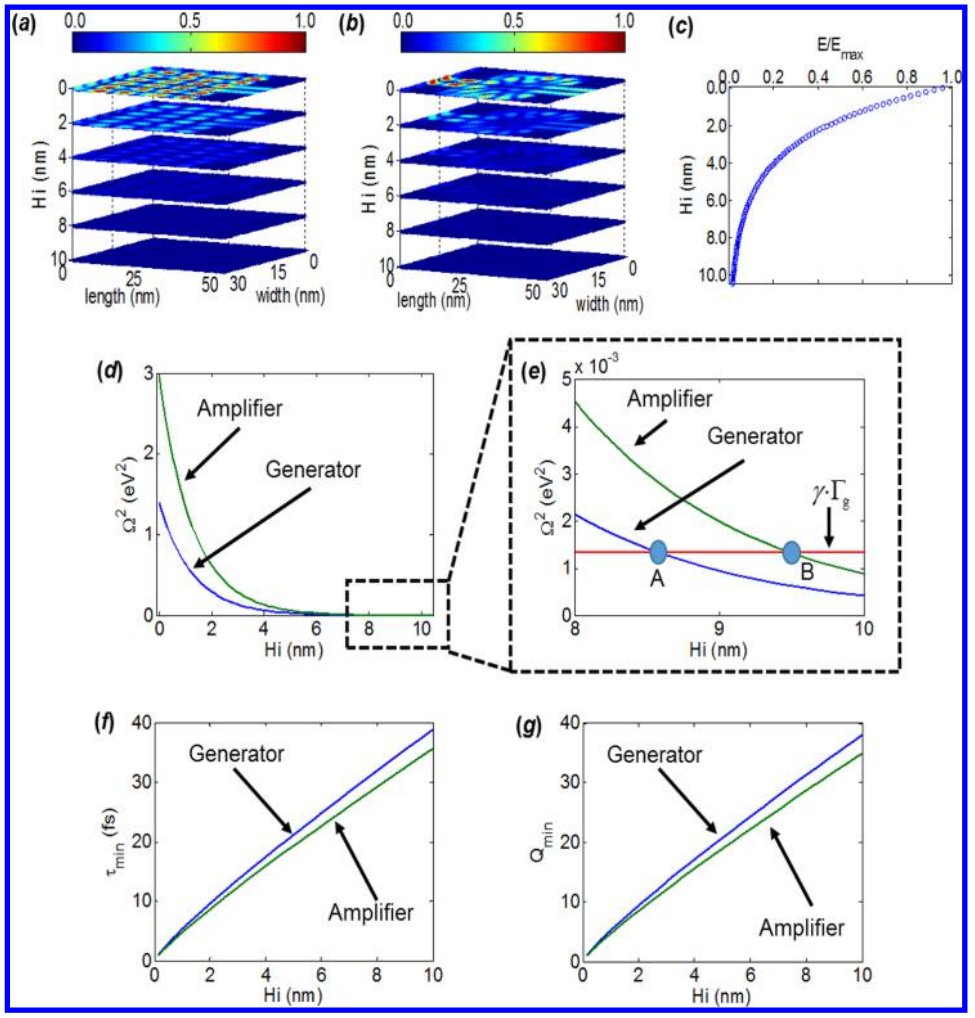

Figure 6. Spatial electric field distribution in electric spaser and spasing conditions, plasmon relaxation time, and quality factor as a function of distance between gain and resonator. (a, b) Spatial distribution of the electric field generated in the electric spaser with a single surface plasmon for cases of generator (a) and amplifier (b). (c) Normalized electric field as a function of the distance between gain and resonator. (d, e) Spasing condition $\Omega^2 > \gamma\Gamma_g$ as a function of the distance between gain and resonator for cases of generator and amplifier. (f, g) Minimum requirement of plasmon relaxation time (f) and quality factor (g) as a function of the distance between gain and resonator for cases of generator and amplifier.

which is near the Dirac cones. As a combined system, the plasmonic mode inside the resonator couples with the gain element spatially and spectrally to initiate and sustain spasing. It is worthy to note that the Figure 5a–f SPP mode patterns also describe the electric field energy distribution in the spaser resonator. Thus they represent the location of the peak electric field in the resonator and gain elements should be placed near the peak to achieve maximum coupling strength.

The composite quantum states of this entire spaser can be defined as the tensor product of the states of the gain element and plamonic subsystem as shown in Figure 2. Since resonance can only take place between the modes in the plasmonic resonator and gain element emission when the condition $E_{12} = E_{sp}$ is satisfied, the plasmonic modes that do not match the gain emission are not considered in the calculation of composite system states. The quantum mechanical model of the carbon-based electric spaser can be built based on the quantization of both the SPP wave modes in the resonator and the gain element.[1−23] The details of the quantization procedure are introduced in the Supporting Information. The time evolution of the quantum states of the electric spaser can be described by the quantum Liouville equation:[1−23]

$$i\hbar\frac{\partial}{\partial t}\rho = [H_{spaser}, \rho] + i\hbar\hat{L}\rho \tag{1}$$

where ρ is the density matrix of the electric spaser system and H_{spaser} is the Hamiltonian of the entire system. $\hat{L}$ is the Lindblad superoperator, which represents the interaction between the spaser system and its environment, such as the dissipation of energy from the spaser to its surroundings and randomization of phase of the quantum states of the spaser system.

Using the density matrix and Lindblad superoperator, the rate equations of the electric spaser system can be obtained as follows:[1−23]

$$\frac{\partial}{\partial t}\rho_{12} = -[\gamma_{co} + i(\omega_{21} - \omega)]\rho_{12} - i\Omega^* a_0^*(\rho_{22} - \rho_{11})$$

$$\frac{\partial}{\partial t}(\rho_{22} - \rho_{11}) = -2i(\Omega a_0\rho_{12} - \Omega^* a_0^*\rho_{21}) - 2\Gamma_{2\to 1}\rho_{22} + 2\Gamma_{1\to 2}\rho_{11}$$

$$\frac{\partial}{\partial t}a_0 = [i(\omega - \omega_{sp}) - \gamma_{sp}]a_0 - i\rho_{12}^*\Omega^* \tag{2}$$

DOI: 10.1021/acsnano.7b06735
ACS Nano 2017, 11, 12573−12582

where ρ_{11}, ρ_{12}, ρ_{21}, and ρ_{22} are the elements of the density matrix, Ω is the single-plasmon Rabi frequency, $\Gamma_{1\to2}$ means the rate of energy pumped into the spaser system, and $\Gamma_{2\to1}$ represents the rate of energy dissipated into the environment. γ_{co} is the decay rate of the coherence terms in the density matrix, and γ_{sp} is the relaxation rate of the selected plasmonic mode. Solving the rate equations provides the static and dynamic characteristics of the electric spaser system.[1−23]

Under stationary assumptions, the condition for spasing can be expressed as[1−23]

$$\frac{(\Gamma_{12}+\gamma_{sp})^2}{(\omega_{12}-\omega_{sp})^2+(\Gamma_{12}+\gamma_{sp})^2}\sum_p |\Omega(p)|^2 \geq \gamma_{sp}\Gamma_{12} \quad (3)$$

where Γ_{12} is the interlevel polarization-relaxation rate and $\omega_{12} = (\varepsilon_2 - \varepsilon_1)/\hbar$ is the interlevel transition frequency for the gain element. At resonance $\omega_{12} = \omega_{sp}$, and when the number of gain elements $p = 1$, the spasing condition reduces to $\Omega^2 \geq \gamma_{sp}\Gamma_{12}$.

In order to investigate whether the spasing condition $\Omega^2 \geq \gamma_{sp}\Gamma_{12}$ can be satisfied in our proposed spaser design, we first evaluate the spatial distribution of the electric field $E_{spatial}$ generated by a single surface plasmon in the resonator with electric field $E_{resonator}$ for both cases of generator and amplifier using the relation $E_{spatial} = E_{resonator} \times \exp(-q \times \mathrm{Hi})$ (q is the wave vector and Hi is the distance away from the resonator), the results of which are shown in Figure 6a and b. It can be observed that the electric field strength decreases as the distance away from the resonator increases. Furthermore, Figure 6c plots the peak value of the normalized electric field strength in the resonator E/E_{max} as a function of the distance away from the resonator Hi using the relation $E/E_{max} = \exp(-q \times \mathrm{Hi})$. It shows that E/E_{max} decreases to below 5% when the distance away from the resonator Hi reaches 10 nm. Then, we place the quantum dot gain element perpendicularly below the peak electric field E_{max} in the resonator to achieve maximum coupling strength and calculate the corresponding Rabi frequency $\Omega = E_{max} \times \exp(-q \times \mathrm{Hi}) \times \mathrm{dg}$. Here, dg is the dipole of the quantum dot gain element; $\mathrm{dg} = e_0 \times d_{cnt}$. d_{cnt} is the diameter of the carbon nanotube. Then the spasing condition $\Omega^2 \geq \gamma_{sp}\Gamma_{12}$ is calculated in Figure 6d and e. Figure 6d presents Ω^2 as a function of the distance between the gain element and the resonator Hi for both spaser generator and amplifier. Figure 6e presents the comparison between Ω^2 and $\gamma_{sp}\Gamma_{12} = \gamma\Gamma_g$. It shows that the spacing condition $\Omega^2 \geq \gamma_{sp}\Gamma_{12}$ is satisfied for the generator when $\mathrm{Hi} < A \approx 8.6$ nm and for the amplifier when $\mathrm{Hi} < B \approx 9.5$ nm. In conventional optical amplifiers and lasers, the threshold for transparency in the amplifiers is lower than the threshold for lasing in the lasers. The details of the exact quantitative analysis of the threshold of Hi for both the spaser generator and amplifier are presented in the sections 4.1−4.7 in Supporting Information.

Next, using the spasing condition $\Omega^2 \geq \gamma_{sp}\Gamma_{12}$, it is straightforward to obtain the spasing threshold of the plasmon relaxation time τ_{min} and plasmon quality factor Q_{min} as a function of the distance between gain element and resonator Hi. Since the relaxation time τ appears in both dispersion relation 4 and plasmon relaxation rate eq 5,[1−23]

$$q \approx \frac{\hbar^2\varepsilon_0(\varepsilon_{r_1}+\varepsilon_{r_2})}{4e^2E_F}\left(1+\frac{i}{\omega\tau}\right)\omega^2 \quad (4)$$

$$\gamma_{sp} = \hbar\omega = \hbar\frac{1}{\tau} = \frac{1.05\times10^{-34}J\cdot s}{\tau} \quad (5)$$

The spasing condition $\Omega^2 \geq \gamma_{sp}\Gamma_{12}$ can be converted to a constraint on τ_{min} and Hi. Figure 6f plots τ_{min} as a function of Hi for spaser generator and amplifier. It shows that, for spasers with larger distance between gain element and resonator, the threshold of plasmon relaxation time needs to be higher to achieve spasing. The threshold of the plasmon quality factor $Q = \omega\tau/2$ is calculated to obtain the minimum limit of quality factor Q_{min} as a function of the distance between gain element and resonator Hi, which is plotted in Figure 6g for both spaser generator and amplifier.

Here, we estimate the terminal (external) input−output characteristics of this spaser prototype. Since the gain element is excited electrically by the source−drain voltage drop, the operating voltage of the spaser U_g can be estimated as $e_0U_g \geq E_{sp} = \hbar\omega_{sp} = 0.46 \times 2.8$ eV for the spaser shown in Figure 5a. E_{sp} and ω_{sp} are the plasmon energy and frequency, respectively, and $e_0 = 1.6 \times 10^{-19}$ C is the elementary electric charge. The operating current can be approximated classically as $I_g \approx U_g/R \approx G \times U_g \approx 0.5 \times 4e_0^2/\mathrm{h} \times 0.46 \times 2.8$ eV$/e_0 \approx 100$ μA, in which, $G = 1/R = 0.5 \times 4e_0^2/h$ is the conductance of the gain element calculated in Figure 4a at the Fermi energy near $0.18E/t$. So the output power of the spaser is estimated as $W_{sp} = I_g \times U_g \approx 130$ μW. From an experimental perspective, the electric spaser prototype we propose here can be realized using common nanofabrication techniques[43−49] ;such as atomic force microscopes and/or scanning electron microscopes[43,44] technology assisted assembly after fabrication of key elements using suitable high-resolution lithography techniques.[45] Silicon dioxide or polydimethylsiloxane can serve as the substrate for the entire spaser system.[47−49] A layer of the substrate material can be deposited between the gain element and the resonator, and a thin layer of dielectric material can be deposited on top of the gain element, using atomic layer deposition or evaporation.[47−49] The carbon nanotube quantum dot can be formed by depositing the top gate contacts on the gate dielectric layer above the gain element, which may complete the fabrication processes.[49] Finally, the whole spaser system can be integrated with external nanoelectronic circuits for applications.[43−49]

CONCLUSION

In essence, we have proposed a carbon based single electron electric spaser in the extreme quantum limit and carried out cavity quantum electrodynamic analysis to evaluate its performance. The main characteristics in our design are that an open resonator is implemented using a graphene nanoribbon and the gain element is made by electrically pumped single carbon nanotube quantum dot. The spasing condition $\Omega^2 \geq \gamma_{sp}\Gamma_{12}$ is examined on this design, and the results show that spasing can be initiated and sustained when the distance between the gain element and the resonator is within certain limits. The limit of distance Hi is calculated in Figure 6e. The limits on plasmon relaxation time and quality factor are concurrently calculated in Figure 6f and g.

The Coulomb blockade effect was observed in our design, which reveals the single-electron-tunneling nature of the gain element.[36−42] In addition, graphene SPP mode field distributions are revealed in the open resonator, which indicates a complicated physical picture of the resonator modes. Moreover, the composite quantum states of the spaser can potentially play a vital role as the quantum bit (qubit) unit including 0 (off) and

DOI: 10.1021/acsnano.7b06735
ACS Nano 2017, 11, 12573−12582

1 (on) states in quantum information processing.[50−54] Finally, in quantum measurement science, our proposed spaser can work as a high-precision plasmon sensor, allowing to count plasmons one by one propagating through the open resonator.[50−54] In this sense, our proposed spaser could be viewed as a multifunctional device.[54]

METHODS

(a) The mode-matching scattering matrix techniques are used to calculate the spatial surface plasmon resonance wave modes by solving the Helmholtz equation in the graphene nanoribbon open resonator. (b) The atomistic basis tight-binding model and NEGF techniques are used to calculate the electron transport properties in the carbon nanotube quantum dot gain medium. (c) The quantum mechanical density matrix approach is employed to calculate the spasing condition. (d) Detailed algorithms and techniques relevant to above methods can be found in the Supporting Information.

ASSOCIATED CONTENT

Supporting Information

The Supporting Information is available free of charge on the ACS Publications website at DOI: 10.1021/acsnano.7b06735.

Mode-matching scattering matrix techniques used to calculate the spatial surface plasmon resonance wave modes by solving the Helmholtz equation in the graphene nanoribbon open resonator; atomistic basis tight-binding model and NEGF techniques used to calculate the electron transport properties in the carbon nanotube quantum dot; quantum mechanical density matrix approach employed to calculate the spasing condition (PDF)

AUTHOR INFORMATION

Corresponding Author

*E-mail: malin.premaratne@monash.edu. Tel: +613 9905 5382. Web: www.ecse.monash.edu.au/staff/malinp.

ORCID

Malin Premaratne: 0000-0002-2419-4431

Notes

The authors declare no competing financial interest.

ACKNOWLEDGMENTS

M.P., B.L., S.D.G., and M.I.S. gratefully acknowledge the financial support from the Australian Research Council Discovery Grant No. DP140100883. W.Z. gratefully acknowledges the National Natural Science Foundation of China (51777168, 61701303), Natural Science Foundation of Shanghai (17ZR1414300), and Shanghai Pujiang Program (17PJ1404100).

REFERENCES

(1) Premaratne, M.; Stockman, M. I. Theory and Technology of Spasers. *Adv. Opt. Photonics* **2017**, *9*, 79−128.

(2) Premaratne, M.; Agrawal, G. P. *Light Propagation in Gain Media: Optical Amplifiers*; Cambridge University Press, 2011; pp 88−112.

(3) Bergman, D. J.; Stockman, M. I. Surface Plasmon Amplification by Stimulated Emission of Radiation: Quantum Generation of Coherent Surface Plasmons in Nanosystems. *Phys. Rev. Lett.* **2003**, *90*, 027402.

(4) Galanzha, E. I.; Weingold, R.; Nedosekin, D. A.; Sarimollaoglu, M.; Nolan, J.; Harrington, W.; Kuchyanov, A. S.; Parkhomenko, R. G.; Watanabe, F.; Nima, Z.; Biris, A. S.; Plekhanov, A. I.; Stockman, M. I.; Zharov, V. P. Spaser as a Biological Probe. *Nat. Commun.* **2017**, *8*, 15528.

(5) Stockman, M. I. Nanoplasmonics: Past, Present, and Glimpse into Future. *Opt. Express* **2011**, *19*, 22029−22106.

(6) Wan, M.; Gu, P.; Liu, W.; Chen, Z.; Wang, Z. Low Threshold Spaser Based on Deep-Subwavelength Spherical Hyperbolic Metamaterial Cavities. *Appl. Phys. Lett.* **2017**, *110*, 031103.

(7) Alix-Panabières, C.; Pantel, K. Biological Labels: Here Comes the Spaser. *Nat. Mater.* **2017**, *16*, 790−791.

(8) Zheng, C.; Jia, T.; Zhao, H.; Zhang, S.; Feng, D.; Sun, Z. Low Threshold Tunable Spaser Based on Multipolar Fano Resonances in Disk−Ring Plasmonic Nanostructures. *J. Phys. D: Appl. Phys.* **2016**, *49*, 015101.

(9) Passarelli, N.; Bustos-Marún, R. A.; Coronado, E. A. Spaser and Optical Amplification Conditions in Gold-Coated Active Nanoparticles. *J. Phys. Chem. C* **2016**, *120*, 24941−24949.

(10) Richter, M.; Gegg, M.; Theuerholz, T. S.; Knorr, A. Numerically Exact Solution of the Many Emitter−Cavity Laser Problem: Application to the Fully Quantized Spaser Emission. *Phys. Rev. B: Condens. Matter Mater. Phys.* **2015**, *91*, 035306.

(11) Parfenyev, V. M.; Vergeles, S. S. Quantum Theory of a Spaser-Based Nanolaser. *Opt. Express* **2014**, *22*, 13671−13679.

(12) Huo, Y. Y.; Jia, T. Q.; Zhang, Y.; Zhao, H.; Zhang, S. A.; Feng, D. H.; Sun, Z. R. Spaser Based on Fano Resonance in a Rod and Concentric Square Ring-Disk Nanostructure. *Appl. Phys. Lett.* **2014**, *104*, 113104.

(13) Zhong, X.-L.; Li, Z.-Y. All-Analytical Semiclassical Theory of Spaser Performance in a Plasmonic Nanocavity. *Phys. Rev. B: Condens. Matter Mater. Phys.* **2013**, *88*, 085101.

(14) Huang, Y. W.; Chen, W. T.; Wu, P. C.; Fedotov, V. A.; Zheludev, N. I.; Tsai, D. P. Toroidal Lasing Spaser. *Sci. Rep.* **2013**, *3*, 1237.

(15) Baranov, D. G.; Vinogradov, A. P.; Lisyansky, A. A.; Strelniker, Y. M.; Bergman, D. J. Magneto-Optical Spaser. *Opt. Lett.* **2013**, *38*, 2002−2004.

(16) Noginov, M. A.; Zhu, G.; Belgrave, A. M.; Bakker, R.; Shalaev, V. M.; Narimanov, E. E.; Stout, S.; Herz, E.; Suteewong, T.; Wiesner, U. Demonstration Of A Spaser-Based Nanolaser. *Nature* **2009**, *460*, 1110−1112.

(17) Stockman, M. I. The Spaser as a Nanoscale Quantum Generator and Ultrafast Amplifier. *J. Opt.* **2010**, *12*, 024004.

(18) Rupasinghe, C.; Rukhlenko, I. D.; Premaratne, M. Spaser Made of Graphene and Carbon Nanotubes. *ACS Nano* **2014**, *8*, 2431−2438.

(19) Apalkov, V.; Stockman, M. I. Proposed Graphene Nanospaser. *Light: Sci. Appl.* **2014**, *3*, e191.

(20) Jayasekara, C.; Premaratne, M.; Stockman, M. I.; Gunapala, S. D. Multimode Analysis of Highly Tunable, Quantum Cascade Powered, Circular Graphene Spaser. *J. Appl. Phys.* **2015**, *118*, 173101.

(21) Berman, O. L.; Kezerashvili, R. Y.; Lozovik, Y. E. Graphene Nanoribbon Based Spaser. *Phys. Rev. B: Condens. Matter Mater. Phys.* **2013**, *88*, 235424.

(22) Paudel, H. P.; Apalkov, V.; Stockman, M. I. Three-Dimensional Topological Insulator Based Nanospaser. *Phys. Rev. B: Condens. Matter Mater. Phys.* **2016**, *93*, 155105.

(23) Li, D.; Stockman, M. I. Electric Spaser in the Extreme Quantum Limit. *Phys. Rev. Lett.* **2013**, *110*, 106803.

(24) Lewenkopf, C.; Mucciolo, E. The Recursive Green's Function Method for Graphene. *J. Comput. Electron.* **2013**, *12*, 203−231.

(25) Liu, B.; Akis, R.; Ferry, D. K. Conductance Fluctuations in Semiconductor Nanostructures. *J. Phys.: Condens. Matter* **2013**, *25*, 395802.

(26) Usuki, T.; Saito, M.; Takatsu, M.; Kiehl, R. A.; Yokoyama, N. Numerical Analysis of Ballistic-Electron Transport in Magnetic Fields by Using a Quantum Point Contact and a Quantum Wire. *Phys. Rev. B: Condens. Matter Mater. Phys.* **1995**, *52*, 8244.

(27) Liu, B.; Akis, R.; Ferry, D. K. Conductance Fluctuations in Graphene Nanoribbons. *J. Comput. Electron.* **2014**, *13*, 950−959.

(28) Akis, R.; Ferry, D. K. Use of the Scattering Matrix for Device Simulations. *J. Comput. Electron.* **2013**, *12*, 356−362.

(29) Liu, B.; Akis, R.; Ferry, D. K. Conductance Fluctuations in Graphene Subjected to Short-Range Disorder. *J. Vac. Sci. Technol., B: Nanotechnol. Microelectron.: Mater., Process., Meas., Phenom.* **2015**, *33*, 04E101.
(30) Usuki, T.; Takatsu, M.; Kiehl, R. A.; Yokoyama, N. Numerical Analysis of Electron-Wave Detection by a Wedge-Shaped Point Contact. *Phys. Rev. B: Condens. Matter Mater. Phys.* **1994**, *50*, 7615−7625.
(31) Liu, B.; Akis, R.; Ferry, D. K.; Bohra, G.; Somphonsane, R.; Ramamoorthy, H.; Bird, J. P. Conductance Fluctuations in Graphene in the Presence of Long-Range Disorder. *J. Phys.: Condens. Matter* **2016**, *28*, 135302.
(32) Akis, R.; Ferry, D. K.; Bird, J. P. Magnetotransport Fluctuations in Regular Semiconductor Ballistic Quantum Dots. *Phys. Rev. B: Condens. Matter Mater. Phys.* **1996**, *54*, 17705.
(33) Laird, E. A.; Kuemmeth, F.; Steele, G.; Grove-Rasmussen, K.; Nygård, J.; Flensberg, K.; Kouwenhoven, L. P. Quantum Transport in Carbon Nanotubes. *Rev. Mod. Phys.* **2015**, *87*, 703−764.
(34) Castro Neto, A. H.; Guinea, F.; Peres, N. M. R.; Novoselov, K. S.; Geim, A. K. The Electronic Properties of Graphene. *Rev. Mod. Phys.* **2009**, *81*, 109−162.
(35) Blum, K. *Density Matrix Theory and Applications*; Springer, 2010.
(36) Livermore, C.; Crouch, C. H.; Westervelt, R. M.; Campman, K. L.; Gossard, A. C. The Coulomb Blockade in Coupled Quantum Dots. *Science* **1996**, *274*, 1332−1335.
(37) Feng, J.; Liu, K.; Graf, M.; Dumcenco, D.; Kis, A.; Ventra, M. D.; Radenovic, A. Observation of Ionic Coulomb Blockade in Nanopores. *Nat. Mater.* **2016**, *15*, 850−855.
(38) Song, Y.; Xiong, H.; Jiang, W.; Zhang, H.; Xue, X.; Ma, C.; Ma, Y.; Sun, L.; Wang, H.; Duan, L. Coulomb Oscillations in a Gate-Controlled Few-Layer Graphene Quantum Dot. *Nano Lett.* **2016**, *16*, 6245−6251.
(39) Xiang, D.; Wu, J.; Gordon, R. Coulomb Blockade Plasmonic Switch. *Nano Lett.* **2017**, *17*, 2584−2588.
(40) Amasha, S.; Rau, I. G.; Grobis, M.; Potok, R. M.; Shtrikman, H.; Goldhaber-Gordon, D. Coulomb Blockade in an Open Quantum Dot. *Phys. Rev. Lett.* **2011**, *107*, 216804.
(41) Akai-Kasaya, M.; Okuaki, Y.; Nagano, S.; Mitani, T.; Kuwahara, Y. Coulomb Blockade in a Two-Dimensional Conductive Polymer Monolayer. *Phys. Rev. Lett.* **2015**, *115*, 196801.
(42) Higginbotham, A. P.; Kuemmeth, F.; Larsen, T. W.; Fitzpatrick, M.; Yao, J.; Yan, H.; Lieber, C. M.; Marcus, C. M. Antilocalization of Coulomb Blockade in a Ge-Si Nanowire. *Phys. Rev. Lett.* **2014**, *112*, 216806.
(43) Javey, A.; Guo, J.; Wang, Q.; Lundstrom, M.; Dai, H. Ballistic Carbon Nanotube Field-Effect Transistors. *Nature* **2003**, *424*, 654−657.
(44) Song, P.; Zhang, X.-Y.; Sun, M.; Cui, X.-L.; Lin, Y. Synthesis of Graphene Nanosheets *via* Oxalic Acid-Induced Chemical Reduction of Exfoliated Graphite Oxide. *RSC Adv.* **2012**, *2*, 1168−1173.
(45) Graf, A.; Held, M.; Zakharko, Y.; Tropf, L.; Gather, M. C.; Zaumseil, J. Electrical Pumping and Tuning of Exciton-Polaritons in Carbon Nanotube Microcavities. *Nat. Mater.* **2017**, *16*, 911−917.
(46) Javey, A.; Kim, H.; Brink, M.; Wang, Q.; Ural, A.; Guo, J.; McIntyre, P.; McEuen, P.; Lundstrom, M.; Dai, H. High-Kappa Dielectrics for Advanced Carbon-Nanotube Transistors and Logic Gates. *Nat. Mater.* **2002**, *1*, 241−246.
(47) Kim, K. S.; Zhao, Y.; Jang, H.; Lee, S. Y.; Kim, J. M.; Kim, K. S.; Ahn, J.-H.; Kim, P.; Choi, J.-Y.; Hong, B. H. Large-Scale Pattern Growth of Graphene Films for Stretchable Transparent Electrodes. *Nature* **2009**, *457*, 706−710.
(48) Zhou, Y.; Loh, K. P. Making Patterns on Graphene. *Adv. Mater.* **2010**, *22*, 3615−3620.
(49) Zhang, Q.; Huang, J.-Q.; Qian, W.-Z.; Zhang, Y.-Y.; Wei, F. The Road for Nanomaterials Industry: A Review of Carbon Nanotube Production, Post-Treatment, and Bulk Applications for Composites and Energy Storage. *Small* **2013**, *9*, 1237−1265.
(50) Bergquist, J. C.; Hulet, R. G.; Itano, W. M.; Wineland, D. J. Observation of Quantum Jumps in a Single Atom. *Phys. Rev. Lett.* **1986**, *57*, 1699.
(51) Brune, M.; Schmidt-Kaler, F.; Maali, A.; Dreyer, J.; Hagley, E.; Raimond, J. M.; Haroche, S. Quantum Rabi Oscillation: A Direct Test of Field Quantization in a Cavity. *Phys. Rev. Lett.* **1996**, *76*, 1800−1803.
(52) Brune, M.; Hagley, E.; Dreyer, J.; Maître, X.; Maali, A.; Wunderlich, C.; Raimond, J. M.; Haroche, S. Observing the Progressive Decoherence of the ″Meter″ in a Quantum Measurement. *Phys. Rev. Lett.* **1996**, *77*, 4887−4890.
(53) Monroe, C.; Meekhof, D. M.; King, B. E.; Itano, W. M.; Wineland, D. J. Demonstration of a Fundamental Quantum Logic Gate. *Phys. Rev. Lett.* **1995**, *75*, 4714−4717.
(54) Haroche, S. Nobel Lecture: Controlling Photons in a Box and Exploring the Quantum to Classical Boundary. *Rev. Mod. Phys.* **2013**, *85*, 1083−1102.

DOI: 10.1021/acsnano.7b06735
ACS Nano 2017, 11, 12573−12582